Development of a statistical model for cervical cancer cell death with irreversible electroporation in vitro

Yongji Yang[1], Michael A. J. Moser[2], Edwin Zhang[3], Wenjun Zhang[1]*, Bing Zhang[4]*

1 Tumor Ablation Group, Complex and Intelligent Systems Research Center, East China University of Science and Technology, Shanghai, China, **2** Department of Surgery, University of Saskatchewan, Saskatoon, Saskatchewan, Canada, **3** Division of Vascular & Interventional Radiology, Department of Medical Imaging, University of Toronto, Toronto, Ontario, Canada, **4** Biomedical Science and Technology Research Center, School of Mechatronic Engineering and Automation, Shanghai University, Shanghai, China

* chris.zhang@usask.ca (WZ); bingzhang84@shu.edu.cn (BZ)

Abstract

Purpose

The aim of this study was to develop a statistical model for cell death by irreversible electroporation (IRE) and to show that the statistic model is more accurate than the electric field threshold model in the literature using cervical cancer cells in vitro.

Methods

HeLa cell line was cultured and treated with different IRE protocols in order to obtain data for modeling the statistical relationship between the cell death and pulse-setting parameters. In total, 340 in vitro experiments were performed with a commercial IRE pulse system, including a pulse generator and an electric cuvette. Trypan blue staining technique was used to evaluate cell death after 4 hours of incubation following IRE treatment. Peleg-Fermi model was used in the study to build the statistical relationship using the cell viability data obtained from the in vitro experiments. A finite element model of IRE for the electric field distribution was also built. Comparison of ablation zones between the statistical model and electric threshold model (drawn from the finite element model) was used to show the accuracy of the proposed statistical model in the description of the ablation zone and its applicability in different pulse-setting parameters.

Results

The statistical models describing the relationships between HeLa cell death and pulse length and the number of pulses, respectively, were built. The values of the curve fitting parameters were obtained using the Peleg-Fermi model for the treatment of cervical cancer with IRE. The difference in the ablation zone between the statistical model and the electric threshold model was also illustrated to show the accuracy of the proposed statistical model in the representation of ablation zone in IRE.

Conclusions

This study concluded that: (1) the proposed statistical model accurately described the ablation zone of IRE with cervical cancer cells, and was more accurate compared with the electric field model; (2) the proposed statistical model was able to estimate the value of electric field threshold for the computer simulation of IRE in the treatment of cervical cancer; and (3) the proposed statistical model was able to express the change in ablation zone with the change in pulse-setting parameters.

Introduction

Electroporation is defined as the creation of micro/nanopores in the cell membrane by transmembrane voltages leading to an increase in cell membrane permeability. Originally, electroporation was used to treat tumors by creating reversible pores in the cell membranes of cancer cells, through which chemotherapeutic drug or plasmid DNA is delivered into intracellular structures to kill tumor cells—a process called electrochemotherapy (ECT) [1]. Based on ECT, Davalos *et al.* proposed the idea of using irreversible pores in the cell membrane to kill tumor cells [2] (without chemotherapy), which has received much attention in the pre-clinical and clinical studies as a monotherapy for cancer treatment [3–7]. Electroporation that generates unrecoverable pores in the cell membrane is termed irreversible electroporation (IRE), differentiating it from ECT. Specifically, irreversible pores are generated by increasing the transmembrane voltage to a critical threshold using high magnitude electric pulses (hundreds to thousands of V/cm) [2]. Unlike the case of ECT, the cell death that occurs in the process of IRE is due to the permanent membrane lysis and/or loss of homeostasis after the generation of irreversible pores in the cell membrane.

Although IRE was only introduced about a decade ago, many pre-clinical and clinical studies have shown that IRE has great potential for the ablation of different types of tumors. Compared with thermal ablation (e.g., radiofrequency ablation, microwave ablation, and laser ablation), IRE has two unique advantages in the therapy of tumors: (1) no collateral thermal injury, and (2) no heat-sink effect when the ablation occurs near large arteries or veins. The second advantage makes IRE appealing for the treatment of tumors which are located in critical positions (e.g. near a large size of blood vessel or a critical organ), at which the thermal ablation methods are unfavorable [7].

However there are some shortcomings with IRE, for example: (1) tumors larger than 3 cm in diameter are not generally amenable to treatment with IRE, and (2) the heterogeneous ablation in the target treatment zone, which can lead to the tumor recurrence. Our present study aims to address these shortcomings. The general idea was to develop a more accurate mathematical model with which the IRE process can be simulated. This idea is viable, as supported by the literature, e.g., the study to make an optimal pre-clinic IRE treatment planning with a mathematical model [8, 9], optimal design of IRE electrodes [10, 11], and understanding of the synergistic effectiveness of IRE combined with other treatments [3, 12].

An electric field threshold (EFT) model was used to define the difference between the live and dead zones. To the IRE treatment on a particular tumor, the EFT was determined by comparing the dead zone between the computer simulation and the in vivo/in vitro experiment. The value of EFT was defined as the electric field strength that encloses the same or approximate dimension of the dead zone with the experiment. Therefore, in the EFT model, the zones

with the electric field strengths higher than a predefined threshold were considered to be effectively ablated or 'dead', otherwise they were considered to be 'live'.

Nickfarjam *et al.* [10] used an EFT of 900 V/cm to differentiate the live and dead zones by comparing the in vivo measurements and the simulation of IRE for a subcutaneous tumor. Similarly, Jiang et al. [13] used an electric field of 600 V/cm as the value of EFT for prostate cancer, based on the fact that nearly 60% of the tumor area in in vitro experiments is correspondent to the estimated injury zone with a radius of 3 mm electric strength circle. Garcia *et al.* [14] chose to use an electric field of 500 V/cm as the EFT of human brain to calculate the volumes of the dead zones with different pulse strengths. Using a rabbit liver model, Miklavčič *et al.* [15] confirmed that the value of EFT varied from 594 V/cm to 680 V/cm under different electric strengths (860–1360 V) while other pulse-setting parameters were set as constants. According to these previous studies, it is clear that the value of EFT is relevant to not only the tissue type but also the IRE-setting parameters. Therefore, the value of EFT for every IRE protocol applied in a computer simulation must be determined in advance using the corresponding in vitro/in vivo experiments, which will increase the cost and difficulty in the application of computer simulation of IRE treatments. The second shortcoming with the EFT model is that it cannot show all the zones in IRE due to its inability to define the transition zone between the live and dead zones, while the transition zone is a key factor to local recurrence after IRE treatments. Indeed, the EFT model uses a 'black-or-white' judgment criteria or strategy [16], which inherently limits its validity in representing the outcome of IRE.

To solve the problems with the EFT model, Golberg and Rubinsky [17] proposed a statistical model describing the relationship between the pulse number and cell death for the evaluation of tissue ablation in IRE, and showed that the statistical model can predict the tissue destruction more accurately, compared with the EFT model. However, the data of the cell death they used was adopted from the experiments of prostate cancers treated with ECT instead of IRE, so results achieved by their work cannot be generalized to the IRE treatment. Thus, a statistical model describing the relationship between the tumor cell death and the IRE pulse-setting parameters merits further study. Furthermore, the pulse length is another key factor that should be taken into consideration in the statistical model as well.

In the study reported in the present paper, a statistical model was developed, which represents the relationship between the pulse-setting parameters (i.e., the pulse length and the number of pulses) and the cell death with the IRE treatment data on the cervical cancer cell line (i.e., HeLa cell) and to show the superiority of the statistical model to the EFT model by comparing the results obtained from both models.

Materials and methods

Tumor cell culture

Human cervical cancer (HeLa) cell line (purchased from Kingmorn life science, Shanghai, China) was cultured as adherent monolayer in Dulbecco's modified Eagle's medium (DMEM)/High Glucose supplemented with 10% fetal bovine serum and 1% penicillin/streptomycin (PS). The cells were grown in culture at 37˚C in 5% CO2 in a humidified incubator. Following 3-mL phosphate buffered saline (PBS) washes, cells were harvested for passaging (split 1:2 or 1:4) or experiments at a confluence of >80% in 100-mm Petri dishes using a 0.25% GIBCO® trypsin-EDTA solution.

IRE experimental set-up and protocols

After the harvest as above, cells were collected from suspensions by centrifuging them at 1500 r/min for 3 min and supernatant was removed. Cells were then re-suspended in the fresh culture medium as described above to a cell density of $1–4×10^6$ cells/mL. The number

and density of cells were monitored by an automated cell counter (Countstar® BioTech, Shanghai Ruiyu Biotech. Co., Ltd., Shanghai, China) using Trypan blue staining technique. The cell sizes were also measured by the cell counter and the cell microscopic images were captured and processed by its built-in software.

Fig 1 shows the experimental set-up and process of IRE treatment and cell viability assessment. For each IRE protocol, 400 μL of prepared cell suspension was pipetted to an electroporation cuvette (Cuvettes PlusTM 640, Harvard Apparatus, Holliston, MA, USA) with a gap of 4 mm, which was placed in an electric shock chamber (BTX Safety Stand 630B, Harvard Apparatus, Holliston, MA, USA) connected to an IRE pulse generator (BTX ECM 830, Harvard Apparatus, Holliston, MA, USA) for the application of IRE pulses. For the control group, the same amount of prepared cell suspension was pipetted to the cuvette, which was also placed in the chamber for 1–60 seconds without the application of electric pulses. After the IRE treatment, the cell suspension was removed to a well of 48-well plate using pipettes for a 4-h incubation as mentioned above prior to the cell viability assessment (discussed in the section of cell viability assessment). IRE was applied at a room temperature of $20 \pm 1°C$. Cuvettes were washed by 75% alcohol and then rinsed by deionized water for the next IRE application.

The pulse length and the number of pulses were deliberately selected to be investigated for their statistical relationships with the cell death. Electric pulses were administrated with each of four pulse lengths (25, 50, 75, and 100 μs) at the frequency of 1 Hz, which is close to the clinical-used ECG-synchronized frequency [18]. For each pulse length, one, ten, thirty, and sixty pulses were delivered, respectively. For each ten-, thirty-, and sixty-pulse case, the pulse strengths of 200, 400, 600, and 800 V were applied, which correspond to the electric fields of 500, 1000, 1500, and 2000 V/cm, respectively. To make the cell death more obvious, an additional pulse strength of 1800 V (corresponding to the electric field of 4500 V/cm) was also applied in the one-pulse case. For each protocol, the same IRE test was performed in quintuplicate (N = 5).
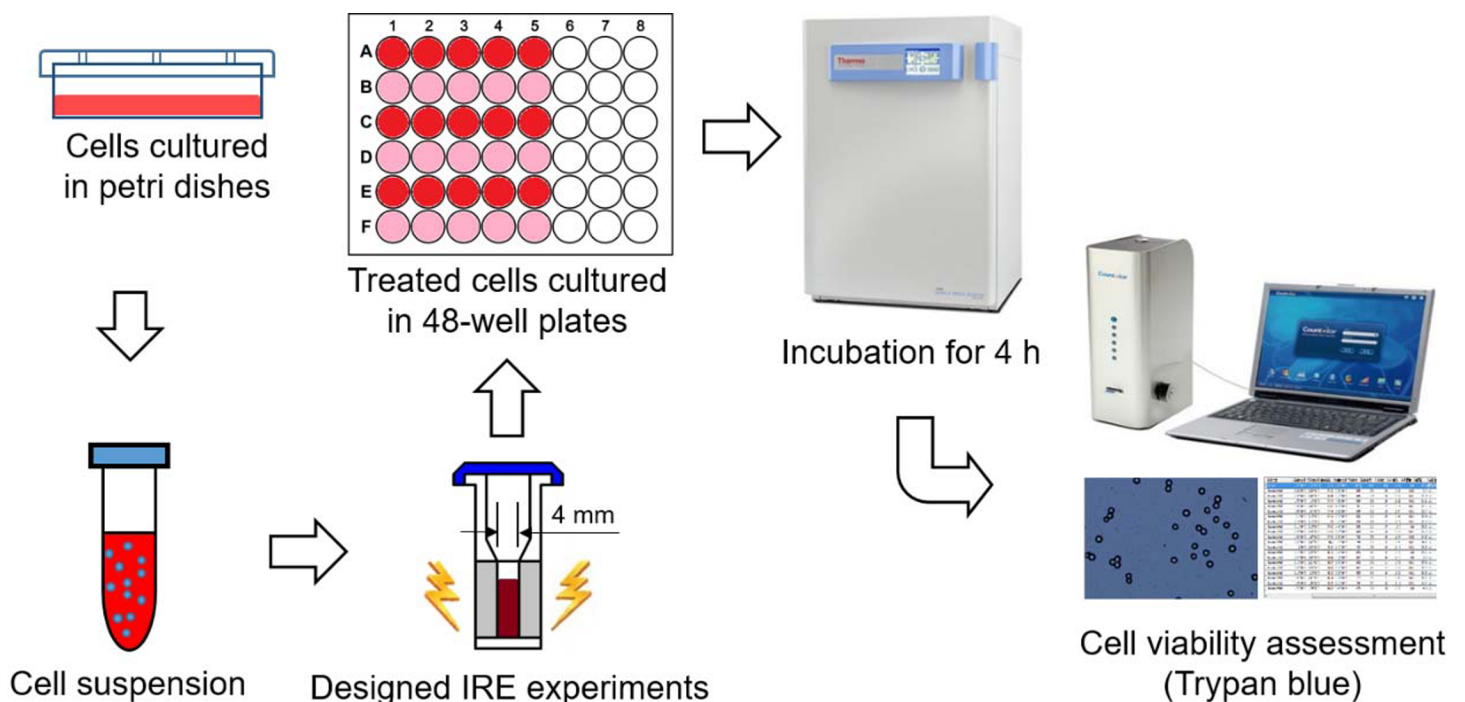

Fig 1. Schematic diagram of IRE experimental set-up and process.

Therefore, a total number of 340 IRE tests were conducted to obtain the cell death data for the statistical modeling in the study.

Cell viability measurement

In the study, cell viability for each IRE experiment (including the control group) was evaluated by the Trypan blue staining technique using the automated cell counter as mentioned above. The blue dye can enter the cell to stain the nucleus blue when the cell membrane is incomplete. However, there are two issues that could affect the accuracy of cell viability measurement, such as the morphology of treated cells that could deceive the cell counter leading to an inaccurate counting and the time of introducing blue dye to the treated cells. As mentioned before, pore formation does not necessarily result in cell death due to the existence of reversible electroporation. So for the classic membrane integrity dye assay, determining the time that the dye being introduced is crucial to the accurate measurement of cell viability. To overcome these two issues, a focused study was conducted to determine the optimal time at which the blue dye should be introduced to most accurately determine cell death. In the present study, the blue dye was introduced to the treated cell suspension at 0-, 0.5-, 1-, 2-, 3-, or 4-h incubation, respectively, after the IRE treatment. All the incubation times were investigated using four groups of IRE pulse-setting parameters: Test 1: pulse strength of 1000 V and 30 pulses, Test 2: pulse strength of 1000 V and 60 pulses, Test 3: pulse strength of 1250 V and 30 pulses, and Test 3: pulse strength of 1250 V and 60 pulses. The other pulse-setting parameters were set as: the pulse frequency of 1 Hz and the pulse length of 100μs. Each experiment in the focused study was also performed in quintuplicate and the result was given as mean ± standard deviation. The one-way ANOVA was employed to assess the statistically significant difference of the results using Minitab 17 (Minitab Inc., State College, PA, USA). Results were considered as statistically significant when P <0.05.

For all tests, the cell viabilities measured at 0-, 1-, and 2-h incubation after IRE treatment by Trypan blue were significantly different (Test 1: P <0.003, P <0.001, and P <0.001, respectively; Test 2: P <0.001, P <0.001, and P <0.002, respectively; Test 3: P <0.001, P = 0.001, and P = 0.001, respectively; and Test 4: P <0.001, P = 0.167, and P <0.01, respectively) as shown in S1 Fig. However, there is no significant difference in cell viability for all tests after 2-h incubation or longer. S2 Fig shows the change of cell morphology after 0-, 1-, 2-, 3-, and 4-h incubation for Test 2. It can be found that with the increase in the incubation time, the cells treated with IRE were clearly distinguishable from those with RE. The treated cells after the 4-h incubation were distinct from the transition phase (no transition cells found). Besides, the cell viability measured after 4-h incubation was quite similar with that achieved by the previous studies under the same pulse-setting conditions for different cell types (HeLa cells: 9.631% ± 2.81% vs. PC3 cells: 27% ± 9% [19] and HeLa cells: 75.93% ± 4.09% vs. DU 145 prostate cancer cells: 80% ± 6% [20]). Therefore, the viability of treated cells was measured by the Trypan blue staining technique after a 4-h incubation after the IRE treatment in the present study.

Statistical model of cell death

Many studies on electroporation to treat the cells in the food industry showed that the death of a heterogeneous population of cells was a statistical event [21–23]. There are many mathematical models proposed in literature to describe the survival of cells due to electroporation, like the first-order kinetics [24], the Peleg-Fermi [25], the Weibull [26], the logistic [27], the adapted Gompertz [28], and the Geeraerd [29] models. Dermol *et al.* conducted a comparison study of several commonly-used statistical models, concluding that the adapted Gompertz and the Geeraerd models are suitable for describing the cell survival as a function of treatment

time, while the Peleg-Fermi, the adapted Gompertz, and the logistic models can all be used as function of electric field for describing cell death due to electroporation.

Thus, considering the number of pulses and the pulse length that are two investigated pulse-setting parameters in the study, the Peleg-Fermi model [25] was used to describe the cell death on the number of pulses and electric field strength for a given pulse length in this study, which was given as:

$$S = \frac{100}{1 + e^{\left(\frac{E-E_c}{A}\right)}}$$

(1)

where, S is the ratio of live cells after the IRE treatment; E (V/cm) is the electric field, E_c is the electric field at which 50% of a population of cells are dead; A (V/cm) is a parameter indicating the steepness of the survival curve at the electric field of E_c. It is worth noting that the exponential function can amplify error. According to the previous studies [25], both $E_c(n,t)$ and $A(n,t)$ as exponential functions of the number of pulses and the pulse duration were also determined by the pulse and the cell types. In the study, the pulse type and the cell type were set as squared wave and HeLa cell, respectively. Both $E_c(n,t)$ and $A(n,t)$ were evaluated at a particular pulse length (t becomes a constant):

$$E_c(n) = E_{c1}e^{-k_1 n} + E_{c2}e^{-k_2 n}$$

(2)

$$A(n) = A_1 e^{-k_3 n} + A_2 e^{-k_4 n}$$

(3)

where E_{c1} (V/cm) and E_{c2} (V/cm) are the electric field at which 50% of a population of cells are dead; A_1 (V/cm) and A_2 (V/cm) are the steepnesses of the survival curve at the electric fields of E_{c1} and E_{c2}, respectively; k_1, k_2, k_3 and k_4 are dimensionless constants; n is the number of pulses.

Or they are evaluated at a particular number of pulses (n becomes a constant):

$$E_c(t) = E_{c3}e^{-k_5 t} + E_{c4}e^{-k_6 t}$$

(4)

$$A(t) = A_3 e^{-k_7 t} + A_4 e^{-k_8 t}$$

(5)

where E_{c3} (V/cm) and E_{c4} (V/cm) are the electric field at which 50% of a population of cells are dead; A_3 (V/cm) and A_4 (V/cm) are the steepnesses of the survival curve at the electric fields of E_{c3} and E_{c4}, respectively; k_5, k_6, k_7 and k_8 are dimensionless constants; and t is the pulse length.

Therefore, the Peleg-Fermi model, Eq (1) can become to Eq (6) or Eq (7) by substituting Eqs (2) and (3) and Eqs (4) and (5), respectively

$$S(E, n) = \frac{100}{1 + e^{\left(\frac{E-E_{c1}e^{-k_1 n}-E_{c2}e^{-k_2 n}}{A_1 e^{-k_3 n}+A_2 e^{-k_4 n}}\right)}}$$

(6)

$$S(E, t) = \frac{100}{1 + e^{\left(\frac{E-E_{c3}e^{-k_5 t}-E_{c4}e^{-k_6 t}}{A_3 e^{-k_7 t}+A_4 e^{-k_8 t}}\right)}}$$

(7)

In present study, Eqs (6) and (7) were applied to build the statistical relationship between the cell death and the number of pulses and the relationship between the cell death and the pulse length, respectively.

Numerical modeling of IRE and EFT model

The electric field distribution during IRE was determined by solving the Laplace equation [14]:

$$-\nabla(\sigma(E)\nabla\varphi) = 0 \tag{8}$$

where φ is the electrical potential; E is the applied electric field; and $\sigma(E)$ is the electric-field-dependent electrical conductivity of the tissue. The relationship between the electric field strength and the electrical conductivity for cervical cancer used in this study was described by using the asymmetrical sigmoid Gompertz curve function [30]:

$$\sigma(E) = \sigma_0 + (\sigma_{max} - \sigma_0)e^{-ae^{(-bE)}} \tag{9}$$

where σ_0 and σ_{max} are the minimum (no electroporation) and maximum (fully saturated) electrical conductivities within a single pulse respectively; a and b that vary with pulse length (t) are unitless coefficients for the displacement and growth rate of the curve, respectively.

$$a = -5 \times 10^{-6}t^2 + 0.004t + 2.803 \tag{10}$$

$$b = -7 \times 10^{-9}t^2 + 5 \times 10^{-6}t + 0.002 \tag{11}$$

For four pulse lengths used in the study, the values of σ_0, σ_{max}, a, and b were tabulated in Table 1. The electric conductivity of healthy cervical tissue is 0.2033 S/m at 1 Hz [31]. In the present study, the electric conductivity of the cervical cancer was determined by increasing the electric conductivity of healthy cervical tissue by the factor of 1.13 [32]. Due to the lack of data, σ_{max} was determined by increasing σ_0 by the factor of 1.8 [33]. Fig 2 shows the electric-field-dependent electrical conductivities of cervical cancer for the four pulses lengths used in the study.

In the present study, a two-dimensional finite element model with a length and width of 100 mm and 80 mm, respectively was used to solve the electric field distribution after the IRE treatment. To avoid the boundary effect, the dimension of the two-dimensional model was determined by a sensitive study. The model was solved in the COMSOL Multiphysics 5.2a (COMSOL, Inc., Burlington, MA, USA) software to get the electric field distribution. The material of this model was set as the cervical cancer tissue. The electric pulses were applied using two 1-mm electrodes with a center-to-center distance of 10 mm acting as the anode and the cathode, respectively.

To solve Eq (8), the electrical boundaries of the electrodes were given as:

$$\varphi = \begin{cases} V_0 & \text{for anode} \\ 0 & \text{for cathode} \end{cases} \tag{12}$$

Table 1. Values of σ_0, σ_{max}, a, and b used in the study.

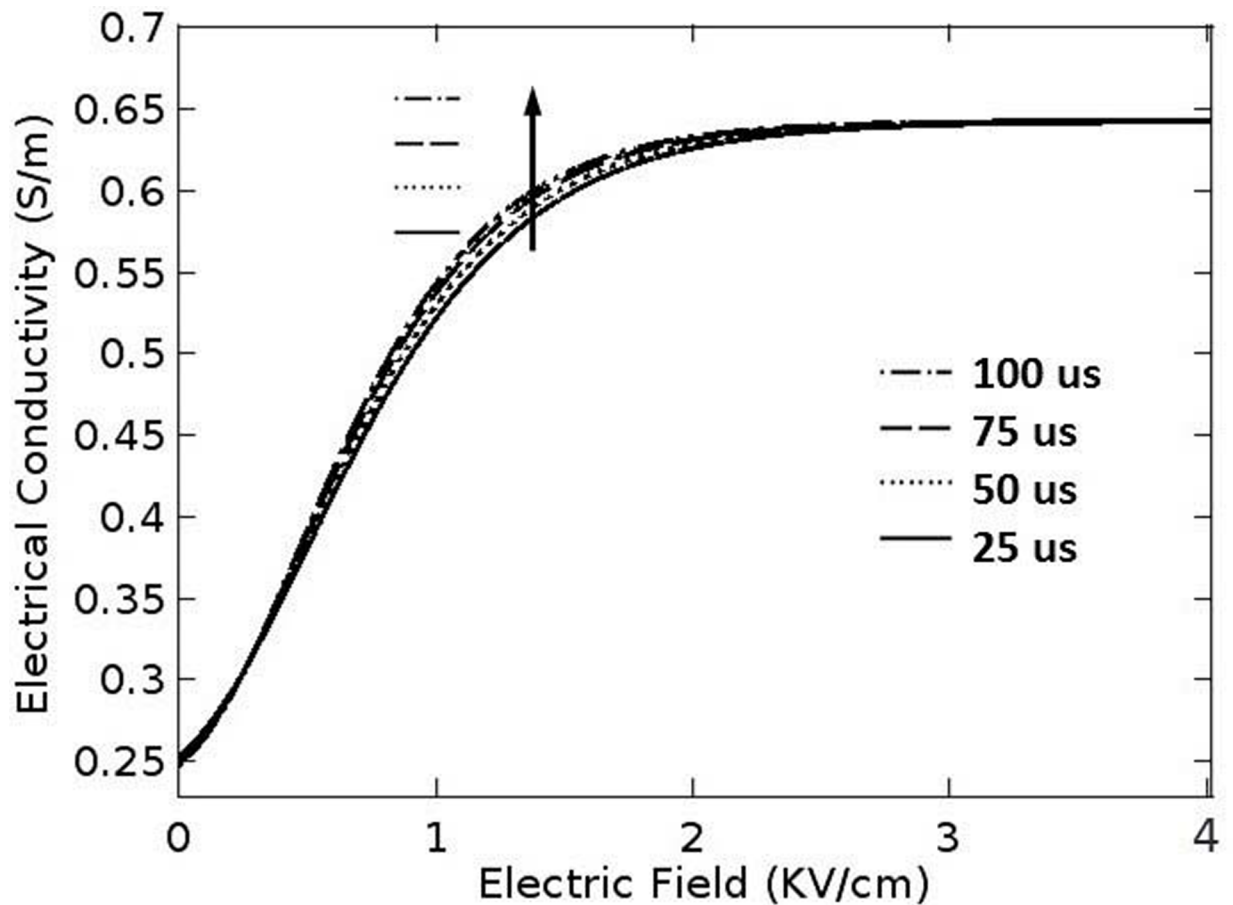| Pulse Length (μs)	σ_0 (S/m)	σ_{max} (S/m)	a	b
25	0.22973	0.64324	2.89988	0.00212
50			2.99050	0.00223
75			3.07487	0.00234
100			3.15300	0.00243

Fig 2. Electric-field-dependent electrical conductivities of cervical cancer for four pulse lengths.

Electrical boundary of the outer surface of tissue was treated as electrically insulated:

$$\frac{\partial \varphi}{\partial n} = 0 \qquad (13)$$

The heat damage was not taken into consideration in the study, though it can be impressive if very high electric pulses are applied, which was not the case in the present study. A convergence test of the finite element model on the number of elements was performed to obtain a stable mesh, which means that the electric field distribution is independent of the number of elements in the study. Eight electric pulses with the pulse strength of 1000 V and the pulse length of 100 μs were applied at the frequency of 1 Hz for the convergence test. Considering the goal of this study was to have an accurate model to calculate the tissue death in IRE treatment, we used the size of ablation zone (EFT model) as an objective item to evaluate the mesh. The value of EFT that leads to death of tissue was set as 600 V/cm. Specifically, the mesh was continually refined until the change of the ablation zone in the model is within 0.1% between the two consecutive meshes. The results of mesh convergence test were given in Fig 3. When the number of elements exceeds 2710, the change in the area of ablation zone was less than 0.1%. Thus, a mesh with 2710 elements was used in the model.
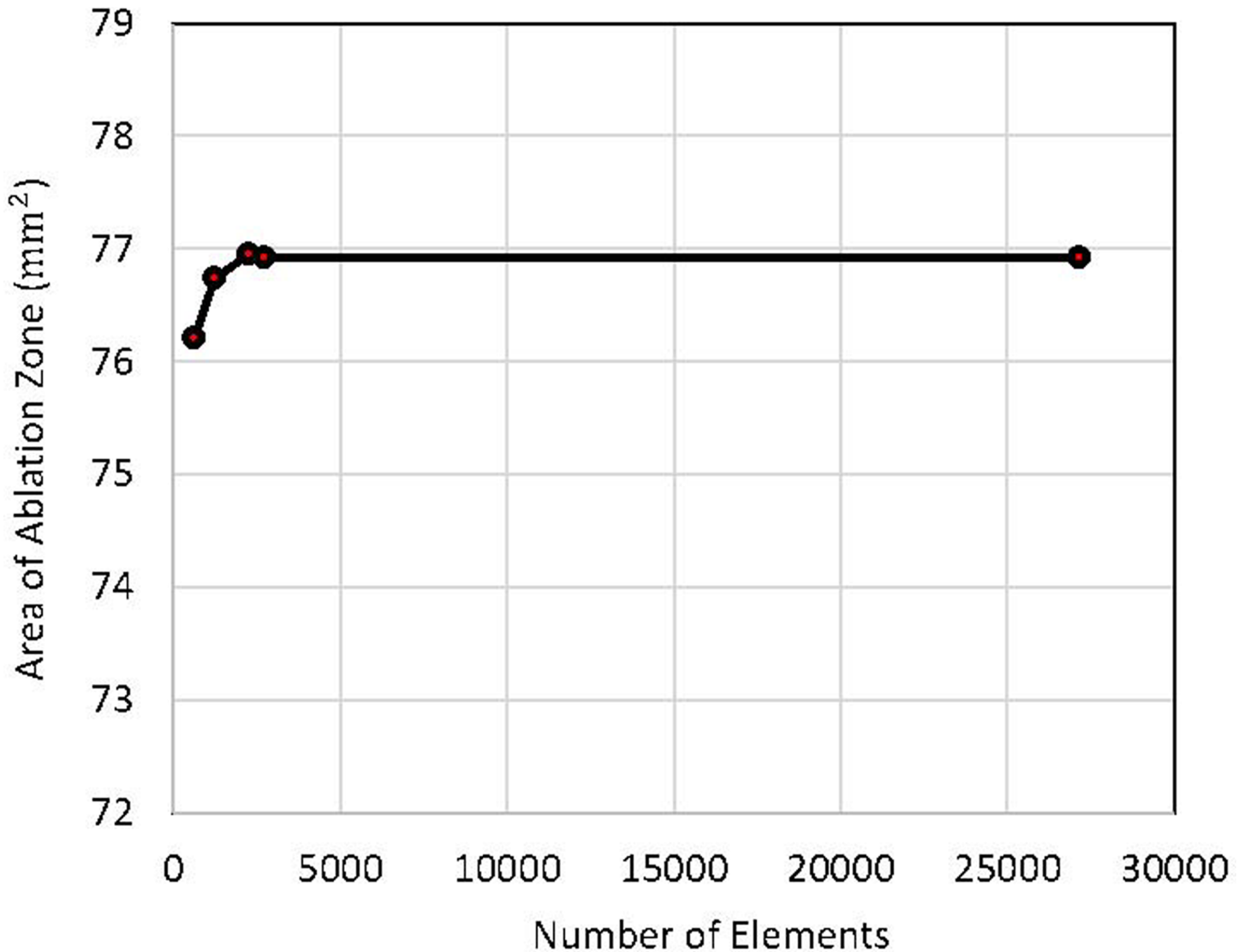
Fig 3. Results of mesh convergence test.

Results

Statistical model of cell death

The viability of HeLa cells treated with different IRE protocols was calculated by comparing with the viability of its control group and given in S1 Table. Fig 4 shows the cell viability dependence on the field strength and the pulse length for each of four-used number of pulses, like 1, 10, 30, and 60 pulses, as shown in Fig 4A, 4B, 4C and 4D, respectively. Fig 5 shows the cell viability dependence on the field strength and the number of pulses for each of four-used pulse length, like 25, 50, 75, and 100 μs, as shown in Fig 5A, 5B, 5C and 5D. The curves shown in Figs 4 and 5 were fitted by the Peleg-Fermi model using Eq (1). It is obvious that the steepness of curves increased with an increase in the pulse strength or the number of pulses, respectively which means the faster ablation effect of IRE.

Based on the data, the curve fitted parameters E_c and A as functions of the number of pulses (n) and the pulse length (t) were estimated and as shown in Fig 6 ($E_c(n)$ and $A(n)$) and Fig 7
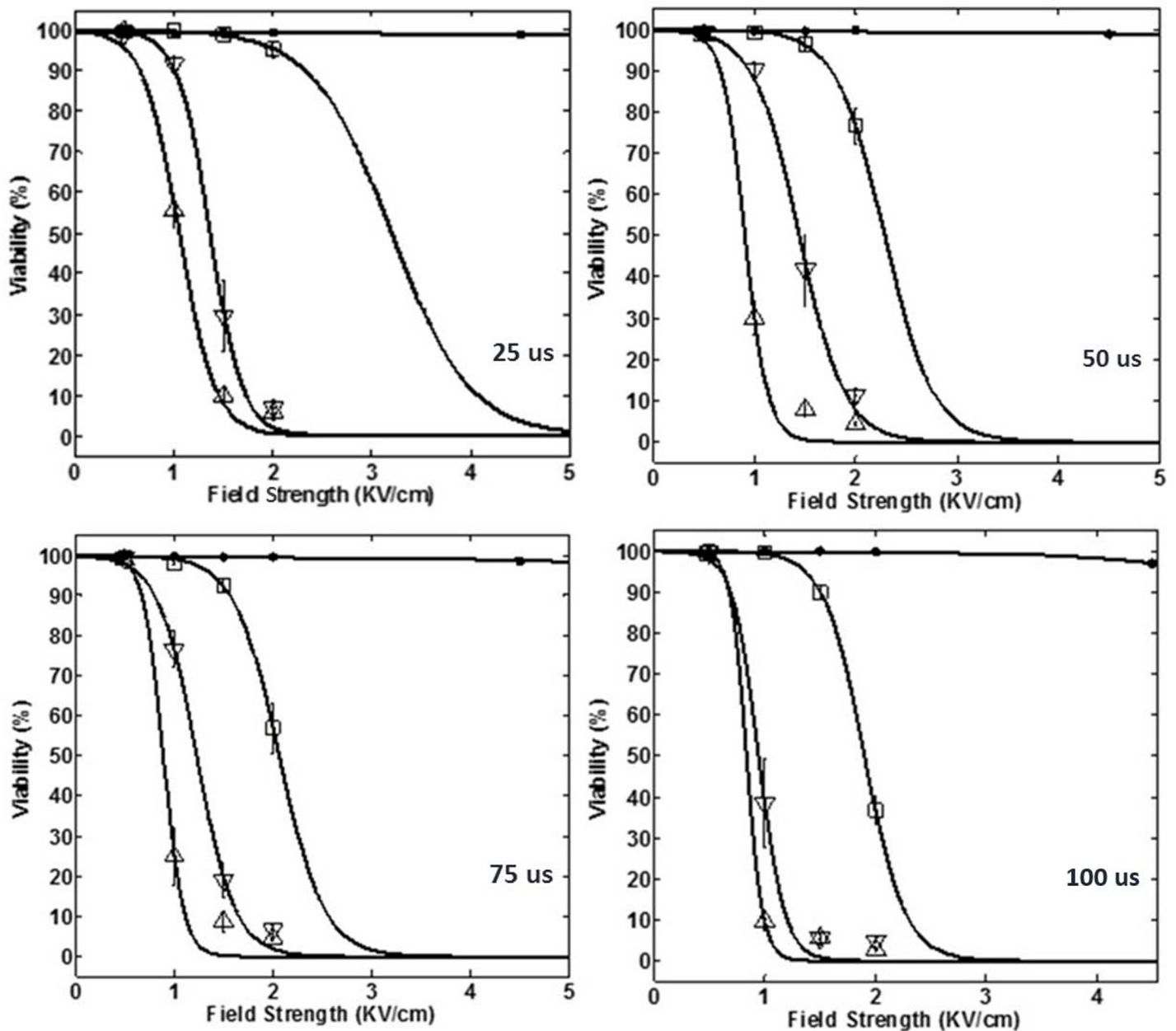
Fig 4. Cell viability dependence on the field strength and each of the four used number of pulses ('●', '□', '▽' and '△' represent 1, 10, 30, and 60 pulses, respectively) at different pulse lengths: a) 25 μs, b) 50 μs, c) 75 μs, and d) 100 μs, respectively.

https://doi.org/10.1371/journal.pone.0195561.g004

($E_c(t)$ and $A(t)$), respectively. The values of fitting parameters for $E_c(n)$ and $A(n)$ as well as $E_c(t)$ and $A(t)$ were tabulated in Tables 2 and 3, respectively. It is noted that, with two exponential components, a very good fitness (see the value of R^2 in Tables 2 and 3) was able to be achieved for both E_c and A (i.e., Eqs (2)–(5)) under each of those pulse length and pulse number conditions. It merits mentioning that the good finesses of E_c and A are critical for the accuracy of cell death in the statistical model of IRE.

It is worth mentioning that the death of treated cells was not getting to zero even though the pulses with high pulse strength were used in the in vitro experiment, which is, we believe,
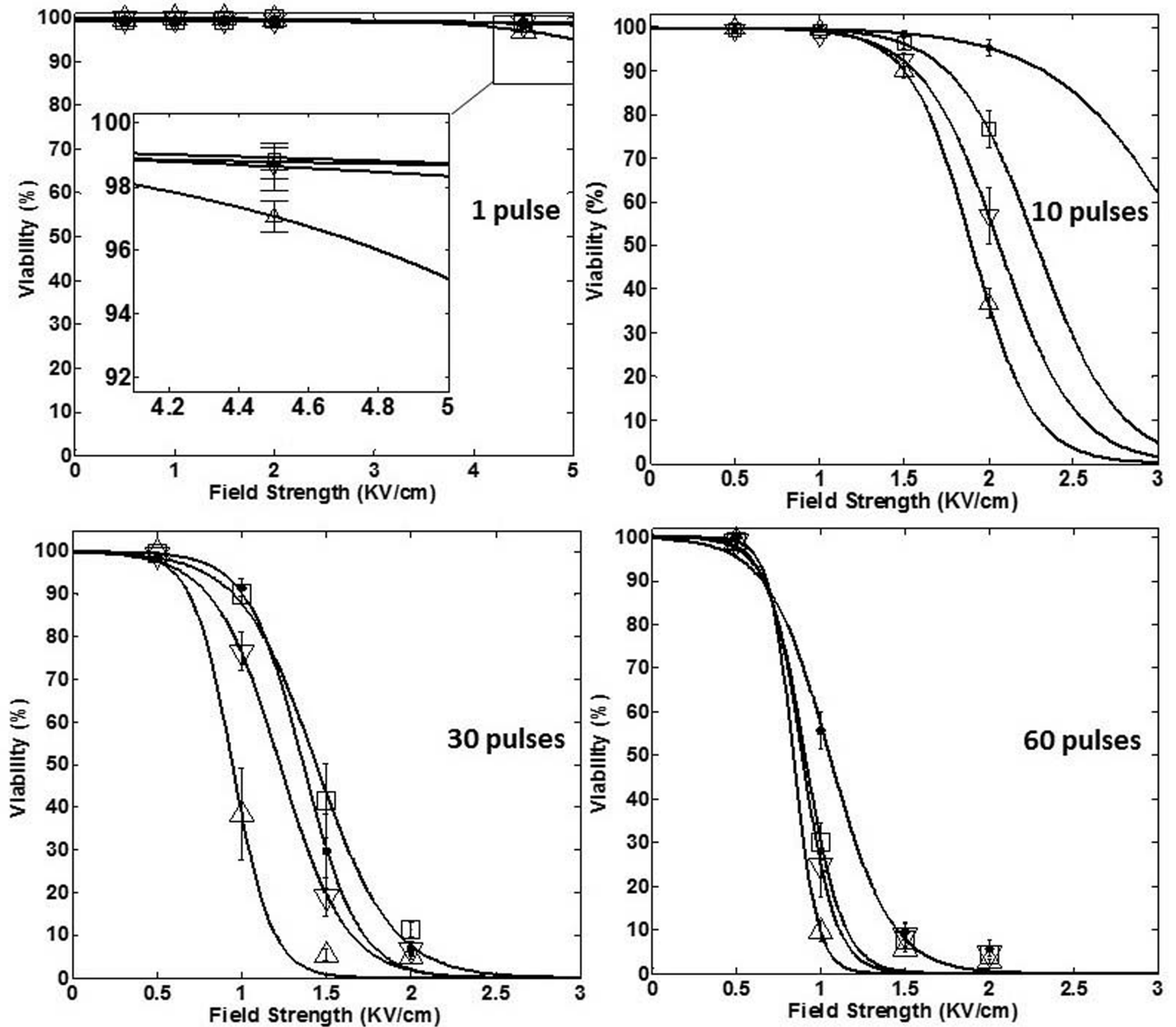
Fig 5. Cell viability dependence on the field strength and each of the four used pulse lengths ('●', '□', '▽' and '△' represent 25, 50, 75, and 100 µs, respectively) for different number of pulses: a) 1, b) 10, c) 30, and d) 60, respectively.

due to the measurement accuracy of the cell counter machine. So in the present study, the cell area with less than 1% viability was taken as dead. Eq (14) was used to calculate the area of ablation zone for the proposed statistical model in the study.

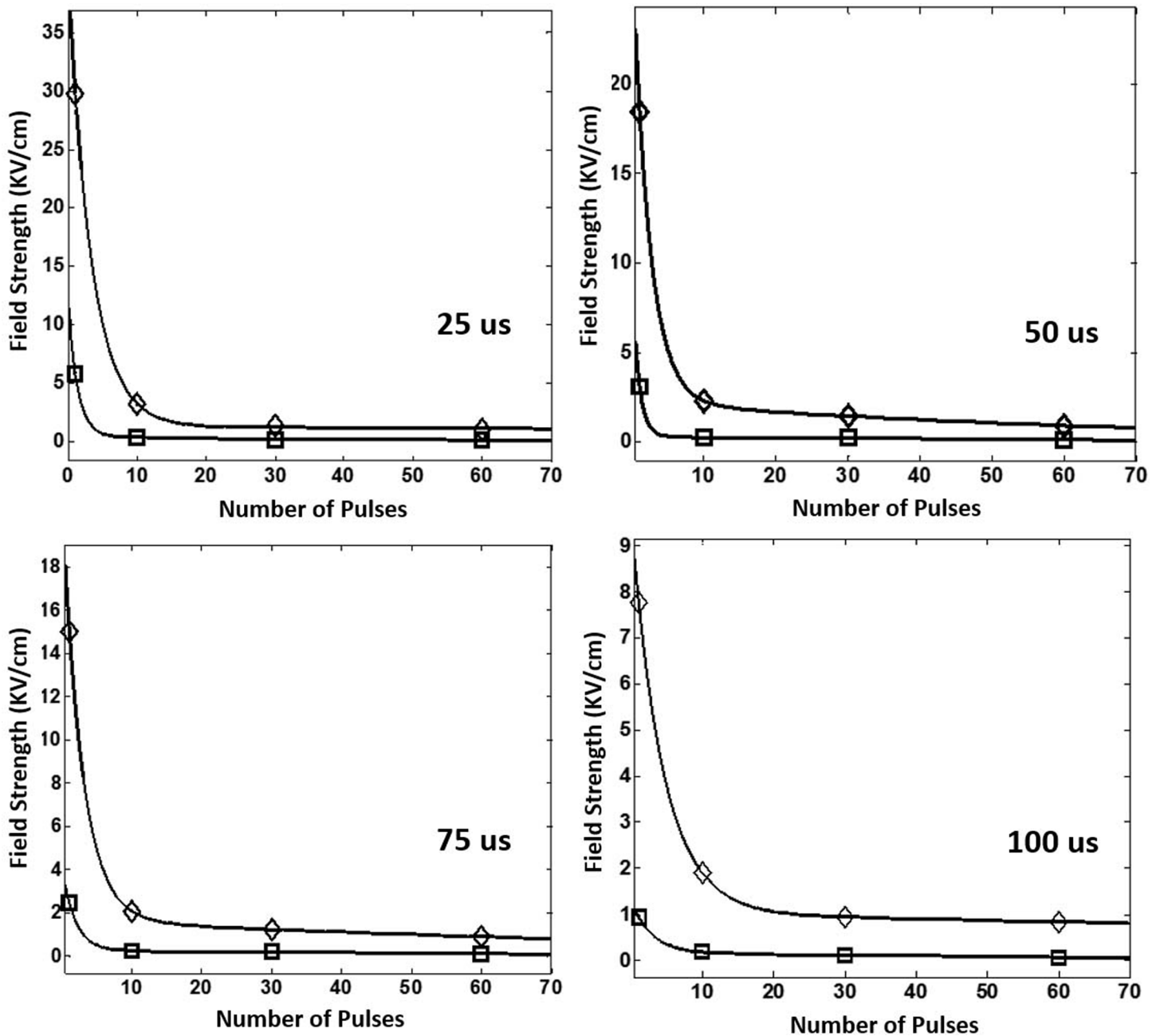$$S = \iint \text{Viability}(x, y) \leq 1\% \, dxdy \tag{14}$$

Fig 6. Dependence of E_c ('◇') and A ('□') on the number of pulses.

Case study

Two case studies were also performed to investigate the accuracy of statistical model in the expression of ablation zone and its applicability for different pulse-setting parameters. Fig 8 shows the comparison of ablation zones between the statistical model and EFT model when 90 pulses with the pulse strength of 2500 V and the pulse length of 100 **μ**s were applied at the frequency of 1 Hz. According to Eq (7), the ablation zone of statistical model was covered by the corresponding electric field of 987 V/cm in the EFT model. It is easy to find that there was a
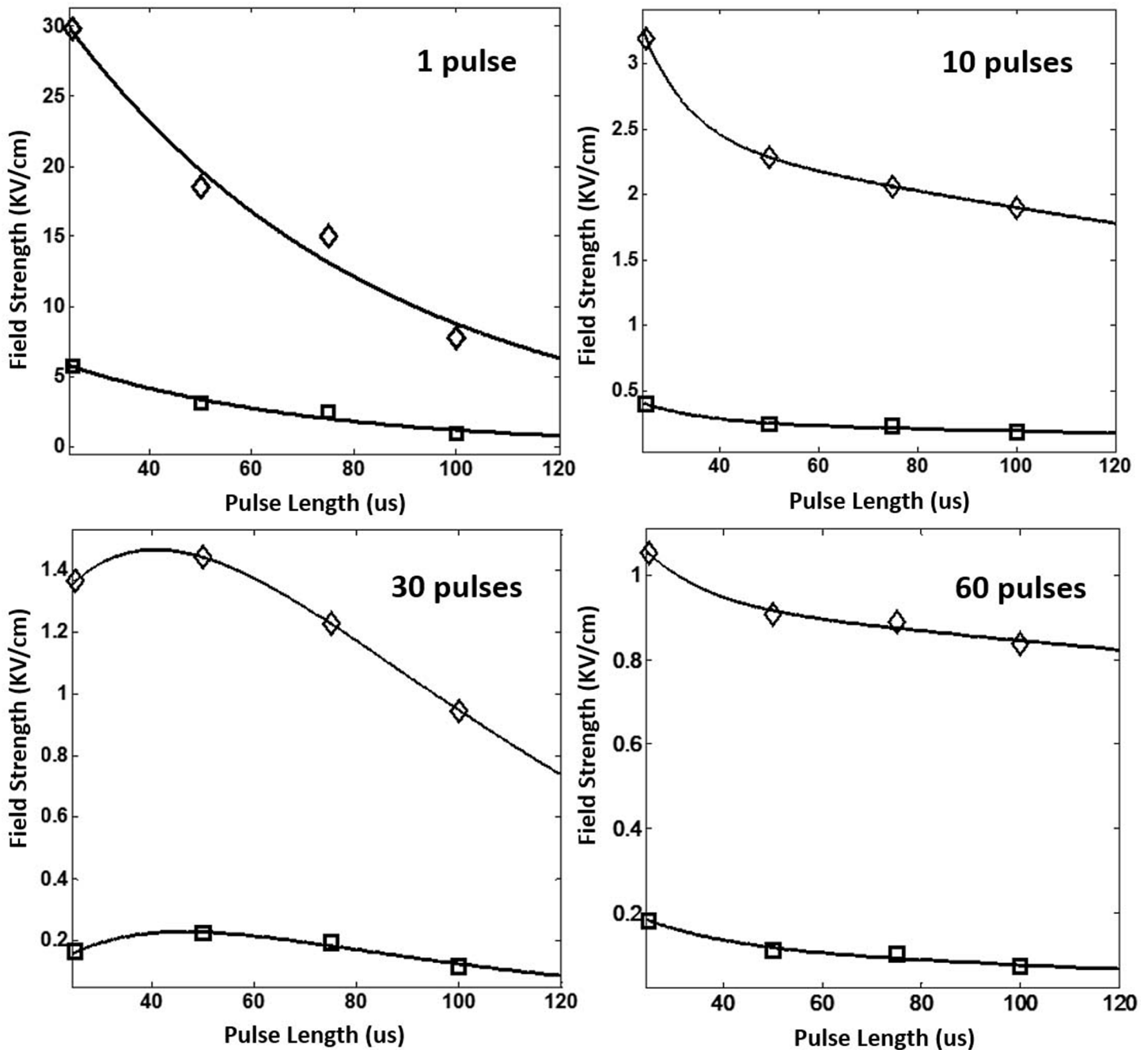
Fig 7. Dependence of E_c ('◇') and A ('□') on the pulse length.

transition zone between the ablation zone and intact zone in the statistical model, which was not able to be found in the EFT model, as shown in Fig 8. Similarly, the values of EFT for the cervical cancer under different pulse-setting parameters were also calculated and tabulated in Table 4. As shown in Table 4, one could find that the value of EFT changes with the IRE-setting parameters, which proves the above-mentioned statement on the disadvantages of EFT model.

Fig 9 shows the changes of ablation zone with the changes in the pulse-setting parameters using the proposed statistical model. A significant increase in the ablation zone was found

Table 2. Curve fitting results for $E_c(n)$ and $A(n)$ at different pulse lengths.

Pulse length (μs)	$E_c(n)$					$A(n)$				
	E_{c1} (V/cm)	K_1	E_{c2} (V/cm)	K_2	R^2	A_1 (V/cm)	K_3	A_2 (V/cm)	K_4	R^2
25	38.310	-0.2953	1.280	-0.001815	1.00	0.4442	-0.02095	11.0300	-0.73010	0.9996
50	24.910	-0.4257	2.250	-0.015030	1.00	0.2916	-0.01354	8.4900	-1.10700	0.9903
75	19.040	-0.3533	1.678	-0.010530	1.00	3.8130	-0.54730	0.2533	-0.01314	0.9998
100	8.428	-0.2237	1.038	-0.003552	1.00	1.0790	-0.33910	0.1678	-0.01329	0.9999

when there was an increase in the pulse strength, the number of pulses, or the pulse length. Fig 9A, 9B and 9C were the ablation zones when the pulse strength was set as to 1000, 2000, and 3000 V, respectively using 60 pulses with the pulse length of 50 μs. Fig 9D, 9E and 9F were the ablation zones when the number of pulses was set as to 30, 60, and 90, respectively using the pulse strength of 2000 V with the pulse length of 50 μs. Similarly, the ablation zone also increased with the increase in the pulse strength, as shown in Fig 9G, 9H and 9I corresponding to the pulse lengths of 10, 50, and 100 μs, respectively. Therefore, it is safe to conclude that the proposed statistical model has the capability of expressing the change of ablation zone with the change in pulse-setting parameters.

Discussion

In present study, a statistical relationship between tumor cell death and the IRE-setting parameters (i.e., pulse length, number of pulses, and pulse strength) was built using the data from HeLa cell suspensions treated with various IRE protocols. The Trypan blue staining technique was used to evaluate the cell viability after each IRE treatment. The time of introducing the Trypan blue dye was also investigated, and it can be concluded that the cell viability of HeLa cells treated with IRE is more accurate and robust when a 4-h incubation is performed before the introduction of dye solution. Due to the lack of data, two different cell types treated with the same IRE protocols with this study were checked for the accuracy of cell viability measured in the study.

As shown in Figs 8 and 9, the treatment process of IRE can be more accurately described by the statistical model comparing with the EFT model. Particularly, the statistical model can demonstrate the transition areas of ablation in which the cells are dying or recovering from pores after the removal of electric field. As shown in Fig 9, it is clear that the transition area of ablation becomes larger and larger with the increase in the pulse strength or the pulse width, which is an important piece of information for surgeons and interventional radiologists when determining the pulse-setting parameters clinically. The accurate determination of the transition area is crucial for preventing local recurrence. The proposed statistical model can be used to facilitate treatment planning for surgeons and interventional radiologists. Unlike the EFT model which uses the experiment to determine the electric threshold for cell death, the

Table 3. Curve fitting results for $E_c(t)$ and $A(t)$ at different numbers of pulses.

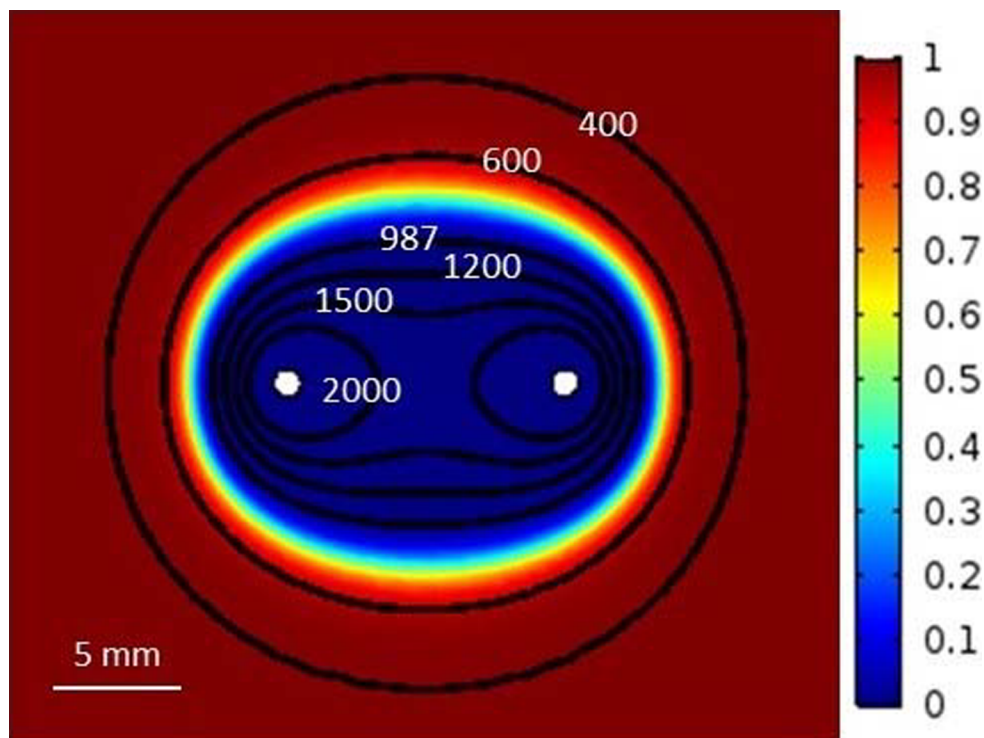| Pulse #	$E_c(t)$					$A(t)$				
	E_{c3} (V/cm)	K_5	E_{c4} (V/cm)	K_6	R^2	A_3 (V/cm)	K_7	A_4 (V/cm)	K_8	R^2
1	44.3000	-0.01620	0	0	0.9760	9.6030	-0.02092	0	0	0.9709
10	11.7700	-0.10880	2.6520	-0.00323	1.0000	1.0010	-0.07780	0.2776	-0.003821	0.9847
30	12.9700	-0.01840	-12.4900	-0.02421	1.0000	3.1940	-0.02519	-3.4880	-0.032750	0.9681
60	0.9476	-0.08218	0.9599	-0.00128	1.0000	0.2557	-0.05917	0.1441	-0.006390	0.9800

Fig 8. Comparison of ablation zones between the statistical model and the EFT model (electric field strength in V/cm).

https://doi.org/10.1371/journal.pone.0195561.g008

statistical model can be easily used to determine the electric thresholds for different IRE protocols. A limitation of this study is that the data used for the statistical model is achieved from the HeLa cells treated with IRE protocols. Experiments with in vivo cervical models treated with IRE would be more realistic for the proposed statistical model. The cell viability can be different between the in vitro and the in vivo experiments because the cell microenvironment can affect the result of IRE treatments. Therefore, in vivo experiments with cervical cancers are still necessary in order to construct a more precise IRE treatment plan that can be used clinically. Also, only cervical cancer cells were used in the study. Future studies are warranted to develop statistical models specific to other cancers commonly treated with IRE, such as prostate cancers, breast cancers, liver cancers, pancreas cancers, etc. However, the overall concept should be similar.

Table 4. Values of EFT for the cervical cancer under different pulse setting parameters.

Pulse strength (V)	Number of pulses	Pulse length (μs)	Pulse frequency (Hz)	Ablation zone (mm²)	Value of EFT (V/cm)
2000	90	100	1	95.115	988
2500	90	100	1	127.780	987
2500	60	100	1	97.978	1186
2500	30	100	1	69.379	1461
2500	90	75	1	125.190	1007
2500	90	50	1	130.380	978
2500	90	25	1	76.248	1397
3000	90	100	1	158.36	987

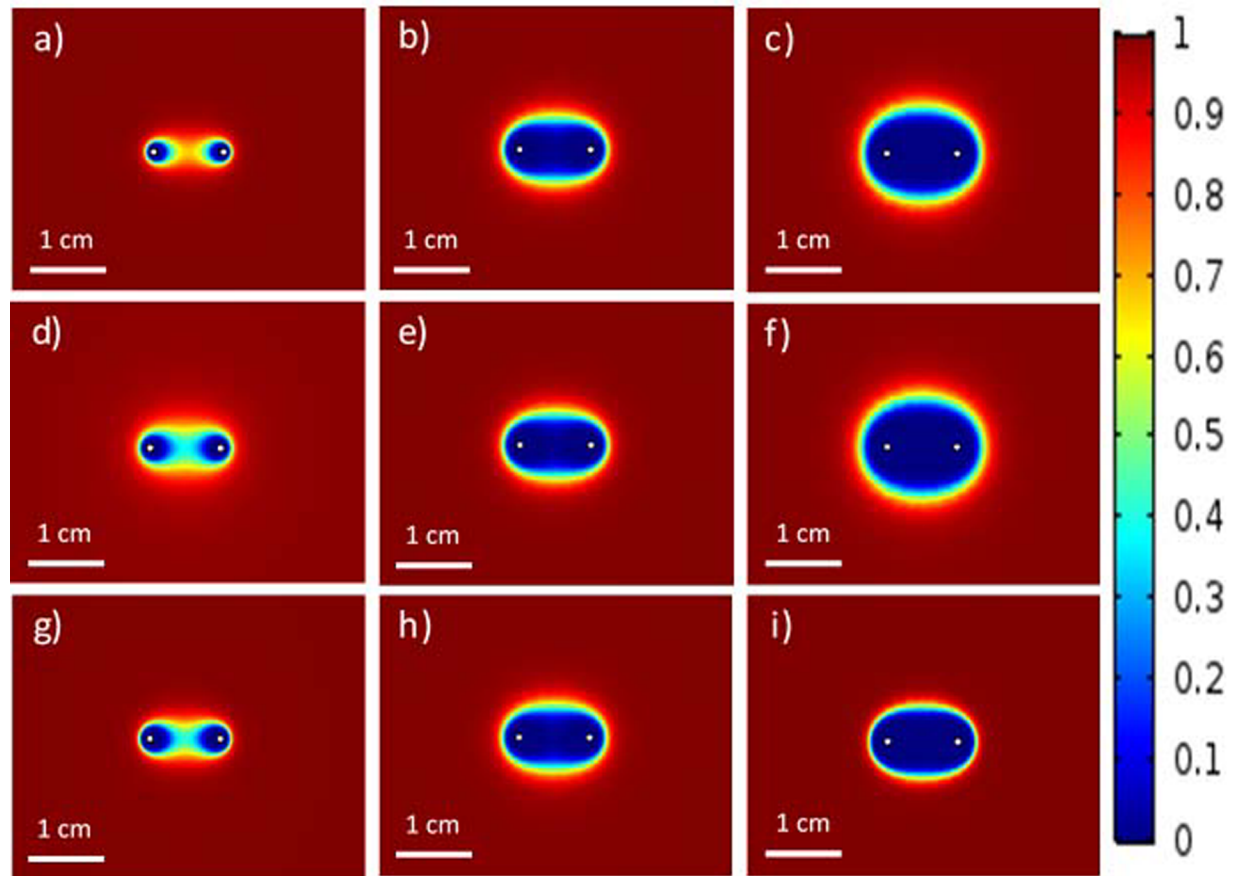https://doi.org/10.1371/journal.pone.0195561.t004

Fig 9. Viability plots for IRE in cervical tumor tissues for different IRE settings regarding to the number of pulses, the pulse strength, and the pulse length: a) 60, 1000 V, and 50 μs, b) 60, 2000 V, and 50 μs, c) 60, 3000 V, and 50 μs, d) 30, 2000 V, and, 50 μs, e) 60, 2000 V, and, 50 μs, f) 90, 2000 V, and 50 μs, g) 60, 2000 V, and 10 μs, h) 60, 2000 V, and 50 μs, and i) 60, 2000 V, and 100 μs, respectively.

https://doi.org/10.1371/journal.pone.0195561.g009

Conclusions

Our conclusions are: (1) the proposed statistical model was able to describe the ablation zone of IRE with cervical cancer cells more accurately compared with the electric field model; (2) the proposed statistical model was able to estimate the value of an electric field threshold for the computer simulation of IRE in the treatment of cervical cancer; and (3) the proposed statistical model was able to express the change of ablation zone with the change in pulse-setting parameters.

Supporting information

S1 Fig. The viabilities of treated HeLa cells at different incubation times in four groups of pulse-setting parameters: a) Test 1, b) Test 2, c) Test 3, and d) Test 4.
(TIF)

S2 Fig. The cell morphology of treated HeLa cells in Test 2 at different measure times: a) 0-h incubation, b) 0.5-h incubation, c) 1-h incubation, d) 2-h incubation, e) 3-h incubation, and f) 4-h incubation. Circle: cells under IRE/RE, blank arrow: live cells, and solid arrow: dead cells.
(TIF)

S1 Table. Relative cell viability dependence on the pulse strength, the number of pulses, and the electric field strength.
(PDF)

Author Contributions

Conceptualization: Bing Zhang.

Data curation: Michael A. J. Moser, Bing Zhang.

Methodology: Bing Zhang.

Supervision: Wenjun Zhang, Bing Zhang.

Validation: Michael A. J. Moser, Edwin Zhang, Bing Zhang.

Writing – original draft: Yongji Yang.

Writing – review & editing: Michael A. J. Moser, Edwin Zhang, Wenjun Zhang, Bing Zhang.

References

1. Yarmush ML, Golberg A, Serša G, Kotnik T, Miklavčič D. Electroporation-based technologies for medicine: principles, applications, and challenges. Annual review of biomedical engineering. 2014; 16.

2. Davalos RV, Mir L, Rubinsky B. Tissue ablation with irreversible electroporation. Annals of biomedical engineering. 2005; 33(2):223–31. PMID: 15771276

3. Shao Q, Liu F, Chung C, Elahi-Gedwillo K, Provenzano PP, Forsyth B, et al. Physical and Chemical Enhancement of and Adaptive Resistance to Irreversible Electroporation of Pancreatic Cancer. Annals of biomedical engineering. 2017:1–12.

4. Yao C, Lv Y, Zhao Y, Dong S, Liu H, Ma J. Synergistic combinations of short high-voltage pulses and long low-voltage pulses enhance irreversible electroporation efficacy. Scientific Reports. 2017; 7 (1):15123. https://doi.org/10.1038/s41598-017-15494-3 PMID: 29123231

5. Paiella S, Butturini G, Frigerio I, Salvia R, Armatura G, Bacchion M, et al. Safety and feasibility of Irreversible Electroporation (IRE) in patients with locally advanced pancreatic cancer: results of a prospective study. Digestive surgery. 2015; 32(2):90–7. https://doi.org/10.1159/000375323 PMID: 25765775

6. Niessen C, Beyer LP, Pregler B, Dollinger M, Trabold B, Schlitt HJ, et al. Percutaneous ablation of hepatic tumors using irreversible electroporation: a prospective safety and midterm efficacy study in 34 patients. Journal of Vascular and Interventional Radiology. 2016; 27(4):480–6. https://doi.org/10.1016/j. jvir.2015.12.025 PMID: 26922979

7. Zhang B, Moser MA, Zhang EM, Xiang J, Zhang W. An In Vitro Experimental Study of the Pulse Delivery Method in Irreversible Electroporation. Journal of Engineering and Science in Medical Diagnostics and Therapy. 2018; 1(1):014501.

8. Yao C, Lv Y, Dong S, Zhao Y, Liu H. Irreversible electroporation ablation area enhanced by synergistic high-and low-voltage pulses. PloS one. 2017; 12(3):e0173181. https://doi.org/10.1371/journal.pone. 0173181 PMID: 28253331

9. Wimmer T, Srimathveeravalli G, Gutta N, Ezell PC, Monette S, Maybody M, et al. Planning irreversible electroporation in the porcine kidney: are numerical simulations reliable for predicting empiric ablation outcomes? Cardiovascular and interventional radiology. 2015; 38(1):182–90. https://doi.org/10.1007/ s00270-014-0905-2 PMID: 24831827

10. Nickfarjam A, Firoozabadi SMP. Parametric study of irreversible electroporation with different needle electrodes: electrical and thermal analysis. International Journal of Hyperthermia. 2014; 30(5):335–47. https://doi.org/10.3109/02656736.2014.937775 PMID: 25144823

11. Yang Y, Moser M, Zhang E, Zhang WC, Zhang B. Optimization of electrode configuration and pulse strength in irrversible electroporation for large ablation volumes without thermal damage. Journal of Engineering and Science in Medical Diagnostics and Therapy. 2018; 1(2).

12. Phillips M, Krishnan H, Raju N, Rubinsky B. Tissue ablation by a synergistic combination of electroporation and electrolysis delivered by a single pulse. Annals of biomedical engineering. 2016; 44(10):3144–54. https://doi.org/10.1007/s10439-016-1624-4 PMID: 27146516

13. Jiang C, Shao Q, Bischof J. Pulse timing during irreversible electroporation achieves enhanced destruction in a hindlimb model of cancer. Annals of biomedical engineering. 2015; 43(4):887–95. https://doi.org/10.1007/s10439-014-1133-2 PMID: 25269611

14. Garcia PA, Rossmeisl JH, Neal RE, Ellis TL, Davalos RV. A parametric study delineating irreversible electroporation from thermal damage based on a minimally invasive intracranial procedure. Biomedical engineering online. 2011; 10(1):34.

15. Miklavčič D, Šemrov D, Mekid H, Mir LM. A validated model of in vivo electric field distribution in tissues for electrochemotherapy and for DNA electrotransfer for gene therapy. Biochimica et Biophysica Acta (BBA)-General Subjects. 2000; 1523(1):73–83.

16. Li J, Zhang W, Yang G, Tu S, Chen X. Thermal-error modeling for complex physical systems: the-state-of-arts review. The International Journal of Advanced Manufacturing Technology. 2009; 42(1–2):168.

17. Golberg A, Rubinsky B. A statistical model for multidimensional irreversible electroporation cell death in tissue. Biomedical engineering online. 2010; 9(1):13.

18. Arena CB, Sano MB, Rossmeisl JH, Caldwell JL, Garcia PA, Rylander MN, et al. High-frequency irreversible electroporation (H-FIRE) for non-thermal ablation without muscle contraction. Biomedical engineering online. 2011; 10(1):102.

19. Rubinsky J, Onik G, Mikus P, Rubinsky B. Optimal parameters for the destruction of prostate cancer using irreversible electroporation. The Journal of urology. 2008; 180(6):2668–74. https://doi.org/10.1016/j.juro.2008.08.003 PMID: 18951581

20. Canatella PJ, Karr JF, Petros JA, Prausnitz MR. Quantitative study of electroporation-mediated molecular uptake and cell viability. Biophysical journal. 2001; 80(2):755–64. https://doi.org/10.1016/S0006-3495(01)76055-9 PMID: 11159443

21. Sale A, Hamilton W. Effects of high electric fields on microorganisms: I. Killing of bacteria and yeasts. Biochimica et Biophysica Acta (BBA)-General Subjects. 1967; 148(3):781–8.

22. Hamilton W, Sale A. Effects of high electric fields on microorganisms: II. Mechanism of action of the lethal effect. Biochimica et Biophysica Acta (BBA)-General Subjects. 1967; 148(3):789–800.

23. Sale A, Hamilton W. Effects of high electric fields on micro-organisms: III. Lysis of erythrocytes and protoplasts. Biochimica et Biophysica Acta (BBA)-Biomembranes. 1968; 163(1):37–43.

24. Bigelow W. The logarithmic nature of thermal death time curves. The Journal of Infectious Diseases. 1921:528–36.

25. Peleg M. A model of microbial survival after exposure to pulsed electric fields. Journal of the Science of Food and Agriculture. 1995; 67(1):93–9.

26. van Boekel MA. On the use of the Weibull model to describe thermal inactivation of microbial vegetative cells. International journal of food microbiology. 2002; 74(1):139–59.

27. Cole MB, Davies KW, Munro G, Holyoak CD, Kilsby DC. A vitalistic model to describe the thermal inactivation ofListeria monocytogenes. Journal of Industrial Microbiology & Biotechnology. 1993; 12(3):232–9.

28. Linton RH. Use of the Gompertz equation to model non-linear survival curves and predict temperature, pH, and sodium chloride effects for Listeria monocytogenes Scott A 1994.

29. Geeraerd A, Herremans C, Van Impe J. Structural model requirements to describe microbial inactivation during a mild heat treatment. International journal of food microbiology. 2000; 59(3):185–209. PMID: 11020040

30. Neal RE II, Garcia PA, Robertson JL, Davalos RV. Experimental characterization and numerical modeling of tissue electrical conductivity during pulsed electric fields for irreversible electroporation treatment planning. IEEE Transactions on Biomedical Engineering. 2012; 59(4):1076–85. https://doi.org/10.1109/TBME.2012.2182994 PMID: 22231669

31. Gabriel C, Gabriel S, Corthout E. The dielectric properties of biological tissues: I. Literature survey. Physics in Medicine and Biology. 1996; 41(11):2231. PMID: 8938024

32. Balidemaj E, De Boer P, van Lier A, Remis R, Stalpers L, Westerveld G, et al. In vivo electric conductivity of cervical cancer patients based on maps at 3T MRI. Physics in medicine and biology. 2016; 61(4):1596. https://doi.org/10.1088/0031-9155/61/4/1596 PMID: 26836010

33. Ivorra A, Al-Sakere B, Rubinsky B, Mir LM. In vivo electrical conductivity measurements during and after tumor electroporation: conductivity changes reflect the treatment outcome. Phys Med Biol. 2009; 54(19):5949. https://doi.org/10.1088/0031-9155/54/19/019 PMID: 19759406